JOURNAL OF GEOPHYSICAL RESEARCH, VOL. 101, NO. D13, PAGES 18,709–18,720, AUGUST 20, 1996

Infrared spectroscopic signatures of $(NH_4)_2SO_4$ aerosols

David D. Weis and George E. Ewing

Department of Chemistry, Indiana University, Bloomington

Abstract. Ammonium sulfate particles in air with average diameters ranging from 0.1 to 0.5-μm have been generated by atomizing aqueous solutions of $(NH_4)_2SO_4$ of various concentrations at ambient temperatures and pressures. The infrared spectra from 4000 to 600 cm^{-1} of the resulting aerosols have been investigated. This spectral region has allowed us to study the four infrared-active vibrational modes of this salt: $\nu_3(NH_4^+)$, $\nu_4(NH_4^+)$, $\nu_3(SO_4^{2-})$, and $\nu_4(SO_4^{2-})$. The frequencies of these modes are similar to published results obtained from infrared studies of the single crystal but are displaced to higher wavenumbers. Depending on relative humidity, the aerosol particles are crystalline or supersaturated aqueous droplets. These phase identifications are possible because liquid water absorption features are found in the droplets but not in the crystals. Extensive Mie theory calculations have been performed for spheres of diameters ranging from 0.1-μm to 2.0-μm to explore frequency shifts and the relative contributions to extinction of scattering and absorption with particle size. We show that, for the smaller particles, the molecular cross section in the $\nu_3(SO_4^{2-})$ region can be used to determine the number of $(NH_4)_2SO_4$ molecules in an aerosol sample. The (small) frequency shifts in this region provide information on the aerosol particle size. A Mie theory calculation of extinction for a model polydisperse aerosol, believed to approximate that of an experimental aerosol, gives reasonable agreement with the observed spectrum. While calculated band centers of the four modes are within 1% of those observed, values of extinction can differ by as much as 50%. We discuss possible reasons for the discrepancies. Spectroscopic changes observed for an aerosol as the particles settle are discussed in terms of kinetic models and Mie theory. We discuss the potential of spectroscopic signatures of tropospheric $(NH_4)_2SO_4$ aerosols for the characterization of their size, morphology, phase, and composition. Finally, we propose a field experiment to measure sulfate aerosol in the arctic troposphere.

Introduction

In recent years, the role of aerosols in many atmospheric processes has received considerable attention. By scattering radiation, aerosols are a significant factor in the Earth's energy balance [*Charlson et al.*, 1992], hence the optical properties of aerosols are important parameters for global climate calculations. Aerosol particles serve as nuclei for the formation of clouds [*Warneck*, 1988]. The activity of aerosol particles in atmospheric chemical reactions is also well known [*Schroeder and Urone*, 1974; *Abbatt and Molina*, 1992; *Hanson and Ravishankara*, 1993; *Vogt and Finlayson-Pitts*, 1994]. The composition and morphology of many types of aerosol particles, such as those in polar stratospheric clouds [*Tolbert*, 1994], have not been determined nor have the chemical roles of the aerosols been fully addressed. At present, there are few in situ techniques that can provide such information; instead, samples must be collected and then transported to a laboratory for analysis. Because particles within aerosols are fragile, they may undergo a variety of physical and chemical changes during the collection process. By contrast, infrared spectroscopy has the potential to answer many questions about the composition, morphology, optical properties, and chemical nature of particles suspended within aerosols.

Particulate $(NH_4)_2SO_4$ in air is an excellent test aerosol for infrared study. This compound has several infrared-active modes which span the IR region from 4000 to 600 cm^{-1}. The hydrogens of NH_4^+ are capable of participating in hydrogen bonds with water, making this ion a potential probe for water-particle interactions. Finally, sulfate is an important constituent of the atmosphere [*Warneck*, 1988] and consequently an understanding of its spectroscopy will prove valuable to environmental scientists.

In this paper we report the results obtained from infrared studies of $(NH_4)_2SO_4$ aerosols under a variety of ambient conditions. While there have been infrared studies of the collected $(NH_4)_2SO_4$ particles of aerosols [*Johnson and Kumar*, 1991] and IR backscatter spectra over a narrow spectral range (1090–920 cm^{-1}) [*Mudd et al.*, 1982], we present here extinction spectra of suspended $(NH_4)_2SO_4$ particles over a broad spectral range (4000–600 cm^{-1}). We also show spectra of aerosols composed of metastable supersaturated aqueous $(NH_4)_2SO_4$ droplets. We have observed changes in band shapes and locations for different size particles under the same atmospheric conditions, for same size particles under different atmospheric conditions, and for aerosols as a function of time. We rely on published optical constants of solid and aqueous $(NH_4)_2SO_4$ and on the results of both Mie theory calculations and particle sedimentation to discuss the observed changes in the spectra of these aerosols. Finally, we propose field measurements of sulfate in the arctic troposphere (arctic haze).

Experiment

A schematic of the experimental apparatus used in this investigation is shown in Figure 1. The aerosols for this study were generated from aqueous solutions of $(NH_4)_2SO_4$ using a commercially available atomizer (TSI Model 3076), specified

Paper number 96JD01543.
0148-0277/96/96JD-01543$09.00

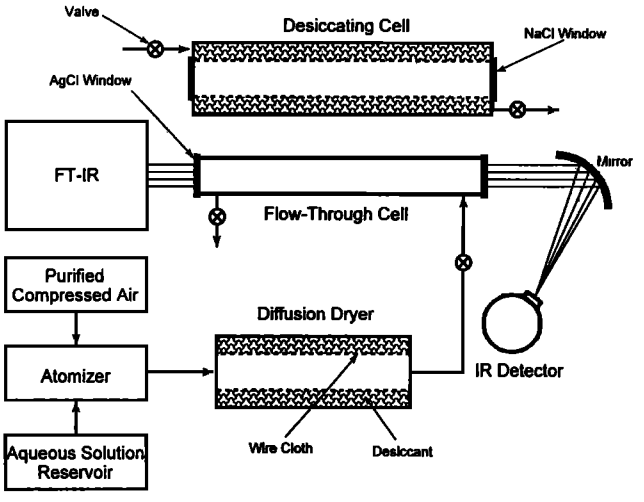

Figure 1. The experimental apparatus. Light from the FT-IR traverses one of two cells containing aerosol and onto a detector. Methods for aerosol preparation are described in the text.

by the manufacturer to generate a lognormal distribution of droplets with a count median diameter, $\bar{d}$, of 0.35-μm, a geometric standard deviation, ζ, of 2.0, and a number density $D_{part} = 10^{14}$ particles m^{-3}. The atomizer is driven by compressed air (Balston 75-62 FT-IR Purge Gas Generator), at a pressure of 350 kPa. The aqueous droplets passed through a diffusion dryer (TSI Model 3062), consisting of a tube of wire cloth surrounded by silica gel desiccant, and into one of the two cells. The flow-through cell is a glass tube of 41 mm diameter and a length of 1 m sealed with rolled AgCl windows (Harshaw-Bicron). The inlet and outlet ports are perpendicular to the cell axis. This cell was used for all flow-through and settling experiments described below. The desiccating cell, similar to the diffusion dryer previously described, consists of a 100-mm- diameter glass tube, 1 m in length, sealed with aluminum caps holding polished NaCl windows (Harshaw-Bicron or Janos). The aerosol region is defined by a 70-mm-diameter tube of 50 mesh stainless steel wire cloth (FP Smith). The region extending from the wire cloth to the cell wall was packed with silica gel. In this cell the inlet and outlet ports are nearly parallel with the cell axis.

Infrared extinction spectra were obtained by directing collimated radiation from a Fourier transform infrared (FT-IR) spectrometer (Nicolet Magna 550) through one of the cells. The light was collected with an off-axis paraboloid mirror and focused onto a detector, with sensing elements of either deuterated triglycine sulfate or liquid nitrogen-cooled mercury cadmium telluride. Each spectroscopic interrogation began with the averaging of from 1 to 1000 interferograms for 4 cm^{-1} resolution. The interferograms were triangle apodized prior to being Fourier transformed. A background spectrum was taken when the cell was flushed with either nitrogen or purified air. The purified air was processed to remove CO_2, H_2O, and CH_4 (Balston 75-62 FT-IR Purge Gas Generator). An aerosol was introduced into the cell and a sample spectrum taken. Spectroscopic data are presented in terms of extinction, $E = \log_{10}(T_b/T_s)$, where T_b is the transmittance of the cell freed of aerosol, and T_s the transmittance of the cell with aerosol. Water vapor absorption in the aerosol spectra, which can obscure extinction by $(NH_4)_2SO_4$ particles, was reduced by subtracting a spectrum of water vapor that had been scaled to match the water vapor in the spectrum of interest.

Three different types of aerosol experiments were conducted. First, in order to obtain spectra at a relative humidity of less than 1% (<1% RH), an aerosol was allowed to flow through the desiccating cell for 3 to 5 min. The flow into and out of the cell was then cut off. Spectra of the aerosol trapped in the cell were then collected 2 - 7 min after stopping the aerosol flow. Second, aerosols were observed in the form they had when they emerged from the diffusion dryer by taking spectra of the aerosols as they passed through the flow-through cell. The flow-through time was of the order of a few seconds while data acquisition required typically 1-5 min. This means that these spectra were averaged over hundreds of samples. This type of experiment produced aerosols at 30±5% RH as measured spectroscopically. Finally, in sedimentation experiments, aerosols were trapped in the flow-through cell just as they were in the desiccating cell. During settling experiments, typically 1-10 scans were averaged to obtain an extinction spectrum. The small number of scans was used to decrease the sampling time. In all of these experiments, background spectra were collected prior to introducing aerosols into the cell or after the cell had been flushed with nitrogen or air for a sufficiently long time to remove all traces of aerosol as determined from extinction spectra taken from the flushed cell.

Since we shall be exploring subtle changes in band centers, $\tilde{\nu}_0$, and bandwidths, Γ (bandwidth at half-height), of spectroscopic features we made use of two curve-fitting

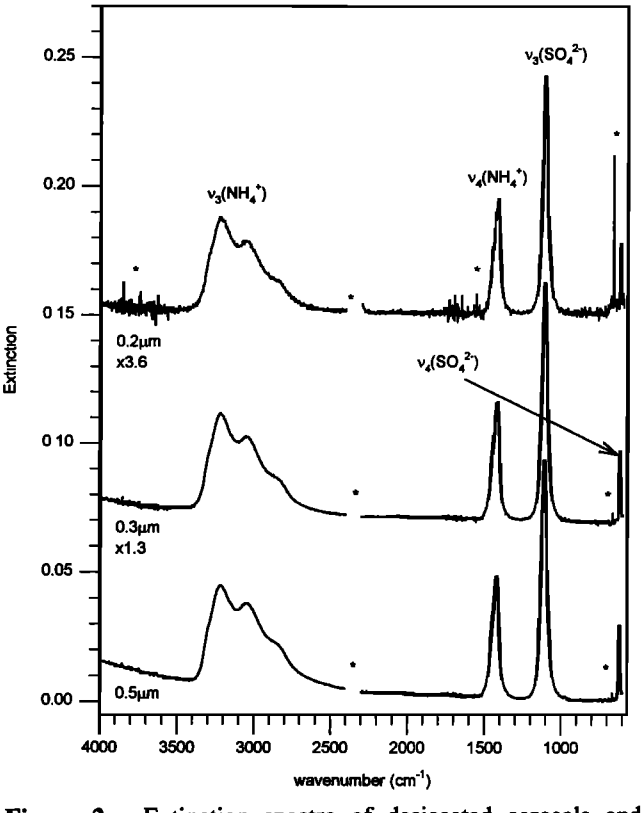

Figure 2. Extinction spectra of desiccated aerosols and spectroscopic assignments of the prominent bands. Diameters of average mass, $d_{\overline{M}}$ (micrometers), are given for each spectrum. The asterisks represent absorption by gas phase H_2O and CO_2. The middle spectrum has been scaled on the extinction axis by a factor of 1.3 and offset by +0.07 extinction units. The upper spectrum has been scaled on the extinction axis by a factor of 3.6 and offset by +0.14 extinction units.

routines. Each band center frequency is determined by least squares fitting of a parabola over the extinction maximum of the features. We have empirically determined that the diffuse spectroscopic features of the $(NH_4)_2SO_4$ particles are well described by lorentzian (rather than say, gaussian) profiles. Consequently, each bandwidth is determined by least squares fitting of a lorentzian function to the extinction profile. Overlapping features can be resolved conveniently into a sum of lorentzian profiles. Parabolic and lorentzian fitting routines are described in the appendix.

Results

Figure 2 shows extinction spectra and spectroscopic assignments for desiccated aerosols prepared from $(NH_4)_2SO_4$ solutions with concentrations of 4.8×10^{-2} kg L^{-1}, 0.11 kg L^{-1}, and 0.71 kg L^{-1} (the saturation limit [*Weast*, 1973]) corresponding to an initial average particle diameter, $d_{\bar{M}}$, of 0.2-μm, 0.3-μm, and 0.5-μm, respectively. The actual average diameter is unknown as the size distribution at any time is a complicated function of both coagulation and sedimentation processes. A justification of these initial average diameter assignments will be given in the following section. Even though these spectra were obtained with the desiccating cell, water vapor subtraction as described in the previous section was used. Water vapor subtraction was necessary because it was impossible to eliminate all of the water from the optical path.

To begin, a glance at Figure 2 shows that the spectroscopic changes among the three initial values of $d_{\bar{M}}$, except for extinction differences, are difficult to distinguish. Thus while the initial particle volumes (proportion to $d_{\bar{M}}^3$) change by over an order of magnitude, the band positions and bandwidths do not appear to change. The only obvious distinction in the three spectra is in the baseline above 3500 cm^{-1}. While the baseline in the 0.2-μm spectrum is essentially flat, it shows a positive curvature for the larger average diameters, being most apparent for the 0.5-μm aerosol.

The modes of NH_4^+ contain structure in their spectroscopic profiles. The $\nu_3(NH_4^+)$ region consists of three overlapping diffuse features and a shoulder. A profile analysis allows these components to be quantified and their band centers, $\tilde{\nu}_0$, and bandwidths, Γ, are listed in Table 1. The band centers of some of these features vary by as much as 10 cm^{-1} for the different average particle diameters. The $\nu_4(NH_4^+)$ mode is composed of two overlapping features with an overall bandwidth roughly one quarter that of ν_3 (NH_4^+). The band centers and bandwidths of the two deconvoluted peaks are within uncertainty limits, invariant to particle diameter.

While the NH_4^+ features are structured, the SO_4^{2-} modes appear to be singlets. As the particle diameter increases, the $\nu_3(SO_4^{2-})$ band center and bandwidth monotonically increases by a few wavenumbers as quantified in Table 1. Because of the sharpness of this band and because it is not obscured by water vapor absorption, we shall focus our attention on the $\nu_3(SO_4^{2-})$ spectroscopic signature in the discussions to follow. The $\nu_4(SO_4^{2-})$ feature profile by contrast is invariant, within experimental uncertainty, to changes in particle diameter.

Figure 3 shows extinction spectra of flow-through aerosols of 0.1-μm, 0.3-μm, and 0.5-μm average particle diameters generated from solutions with concentrations of 5.5×10^{-3} kg L^{-1}, 0.11 kg L^{-1}, and 0.71 kg L^{-1}, respectively. These aerosols were at a relative humidity of 30±5% RH. The differences among the samples is more apparent than for the desiccated aerosols. The baselines in both the 0.3-μm and 0.5-μm spectra show positive curvatures toward higher wavenumbers, while the 0.1-μm spectrum has an essentially flat baseline. The band center and bandwidth values are listed in Table 2.

In addition to the four features observed of ν_3 (NH_4^+) of Figure 2, there is a shoulder at 3450 cm^{-1} in the 0.1-μm and 0.3-μm spectra, but not in the 0.5-μm spectrum. A weak diffuse feature near 1600 cm^{-1} is also apparent in the 0.3-μm spectrum that is absent in the 0.5-μm spectrum. As in the spectra of the desiccated aerosols, $\nu_4(NH_4^+)$ also consists of a pair of overlapping features.

The profile differences in the NH_4^+ bands with ammonium sulfate sampling conditions is emphasized in Figures 4 and 5. In Figure 4 the $\nu_3(NH_4^+)$ region for flow-through and desiccated aerosols is compared with the absorption spectrum of an aqueous solution of $(NH_4)_2SO_4$ [*Remsberg*, 1971]. We shall comment on the extinction differences near 3400 cm^{-1} in

Table 1. Band Centers and Bandwidths of Desiccated $(NH_4)_2SO_4$ Aerosols with Several Average Diameters

	$d_{\bar{M}} = 0.2$ μm		$d_{\bar{M}} = 0.3$ μm		$d_{\bar{M}} = 0.5$ μm	
	$\tilde{\nu}_0$, cm^{-1}	Γ, cm^{-1}	$\tilde{\nu}_0$, cm^{-1}	Γ, cm^{-1}	$\tilde{\nu}_0$, cm^{-1}	Γ, cm^{-1}
$\nu_3(NH_4^+)$	3300[a]	shoulder	3300[a]	shoulder	3300[a]	shoulder
	3219±1[b]	~200	3221±1[c]	~200	3216±0.6[c]	~200
	3062±2[b]	~200	3055±1[c]	~200	3050±1[c]	~200
	2850±10[a]	~200	2850±10[a]	~200	2850±10[a]	~200
$\nu_4(NH_4^+)$	1450±4[d]	46±8[d]	1449±1[d]	48±2[d]	1449±1[d]	46±2[d]
	1472±1[d]	36±2[d]	1421.2±0.4[d]	35±1[d]	1420.7±0.2[d]	37±1[d]
$\nu_3(SO_4^{2-})$	1114.3±0.2[e]	39.5±0.6[f]	1113.8±0.1[e]	42.2±0.6[f]	1112.6±0.2[e]	43.9±0.8[f]
$\nu_4(SO_4^{2-})$	620.5±0.7[f]	14±3[f]	619.5±0.3[f]	15±1[f]	619.6±0.4[f]	15±1[f]

[a]Estimated.
[b]Parabolic fit to points ≥ 80% of peak height.
[c]Parabolic fit to points ≥ 95% of peak height.
[d]Bi-lorentzian fit.
[e]Parabolic fit to points ≥ 90% of peak height.
[f]Lorentzian fit.

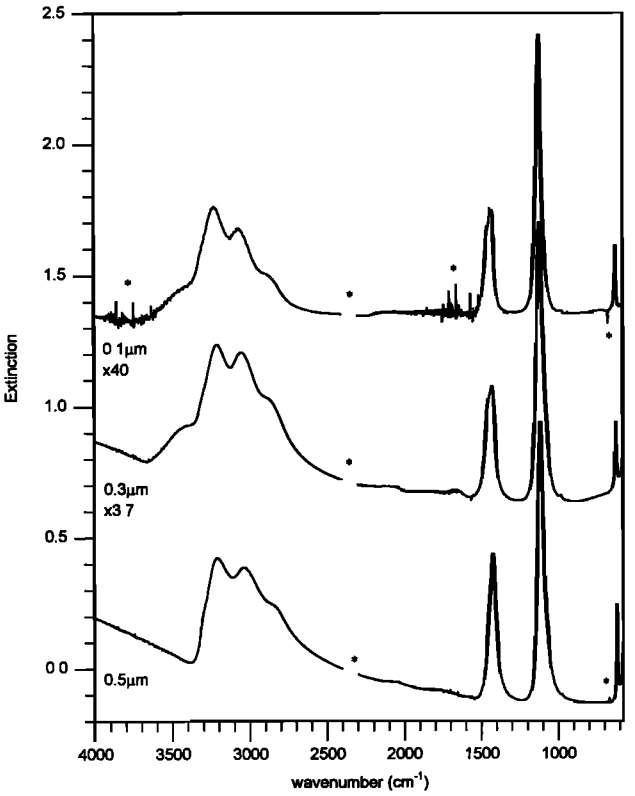

Figure 3. Extinction spectra of flow-through aerosols. Diameters of average mass, $d_{\bar{M}}$ (micrometers), are given for each spectrum. The asterisks represent extinction by gas phase H_2O and CO_2. The middle spectrum has been scaled on the extinction axis by a factor of 3.7 and offset on the extinction axis by +0.8. The top spectrum has been scaled on the extinction axis by a factor of 40 and offset on the extinction axis by +1.4.

discussions to follow. In Figure 5 the high wavenumber doublet component of ν_4 (NH_4^+) dominates in the flow-through aerosol but not in the desiccated sample. This observation will also be discussed later.

The $\nu_3(SO_4^{2-})$ band for the flow-through sample red shifts monotonically by a few wave numbers as the average particle size increases as it did for the desiccated particles; however, the bandwidths for this feature do not follow a clear trend. The ν_3 band of the flow-through aerosols has a trailing edge on the low wavenumber side that is not observed in the spectra of the desiccated aerosols; $\nu_4(SO_4^{2-})$ is again a single band.

Figure 6 shows the results of a sedimentation experiment at 30±5% RH. The aerosol was generated from a 0.11 kg L^{-1} solution of $(NH_4)_2SO_4$ that corresponds to an average initial particle diameter of $d_{\bar{M}}$ = 0.3-μm. The plots show that the integrated extinction (from 1200 to 1000 cm^{-1}) decreases with time and also that the location of the $\nu_3(SO_4^{2-})$ band center shifts to higher wavenumbers with time. (The fluctuation in band center positions in Figure 6 beyond 40 min is the result of the low signal-to-noise ratio as the particle abundance decreased.)

Discussion

Aerosol Particle Size Distributions

Because of their enormous variation in sizes, the size distribution within an aerosol is usually described by its distribution function $dD_{part}/d(\log d)$ versus $\log(d)$ where D_{part} is the particle number density and d is the particle diameter. The maximum of this function locates the count median diameter ($\bar{d}$). When the function is gaussian in form, the distribution is said to be lognormal. The width of the distribution is given by the geometric standard deviation, ζ, defined by [*Hinds*, 1982]

$$\ln(\zeta) = \left[\frac{\sum_{i=1}^{J}\left(\ln d_i - \ln \bar{d}\right)^2}{J-1}\right]^{\frac{1}{2}} \quad (1)$$

where J is the total number of particles and d_i is the diameter of the ith particle. As noted before, our aerosol generator initially produces a lognormal particle distribution with $\bar{d}$ = 0.35-μm and ζ = 2.0.

Table 2. Band Centers and Bandwidths of Flow-Through $(NH_4)_2SO_4$ Aerosols with Several Average Diameters

	$d_{\bar{M}}$ = 0.1 μm		$d_{\bar{M}}$ = 0.3 μm		$d_{\bar{M}}$ = 0.5 μm	
	ν_0, cm^{-1}	Γ, cm^{-1}	ν_0, cm^{-1}	Γ,	ν_0, cm^{-1}	Γ, cm^{-1}
ν_1, ν_3 (H_2O)	3450±10[a]	~200	3450±10[a]	~200	____	____
ν_2 (H_2O)			1650±10[a]	~100	____	____
$\nu_3(NH_4^+)$					3300[a]	shoulder
	3222.2±0.6[e]	~200	3206.0±0.2[c]	~200	3205±1[e]	~200
	3066±1[e]	~200	3050.3±0.2[c]	~200	3036.6±0.4[e]	~200
	2850±10	~200	2850±10	~200	2850±10	~200
$\nu_4(NH_4^+)$	1448±4[d]	60±6[d]	1451±1[d]	57±2[d]	1452.4±0.8[d]	36±2[d]
	1423±1[d]	33±6[d]	1421.3±0.6[d]	41±1[d]	1420.4±0.4[d]	47.6±0.8[d]
$\nu_3(SO_4^{2-})$	1117.1±0.2[e]	39.5±0.8[f]	1112.8±0.1[e]	54±2[f]	1111.1±0.2[e]	47±2[f]
$\nu_4(SO_4^{2-})$	620.9±0.2[f]	14.7±0.8[f]	620.2±0.2[f]	17±1[f]	619.1±0.3[f]	15±1[f]

See footnotes for Table 1.

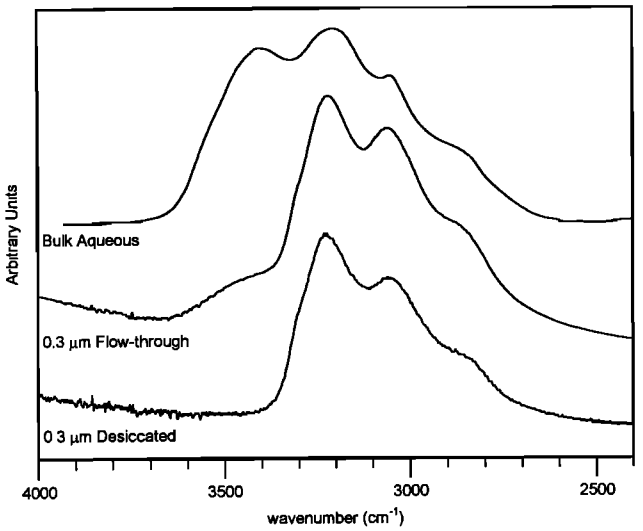

Figure 4. Extinction spectra of a 0.64 kg L^{-1} aqueous solution of $(NH_4)_2SO_4$ taken from data of Remsberg [1971], a 0.3-μm flow-through aerosol, and a 0.3-μm desiccated aerosol. These spectra were normalized to have the same band height and then offset on the vertical axis.

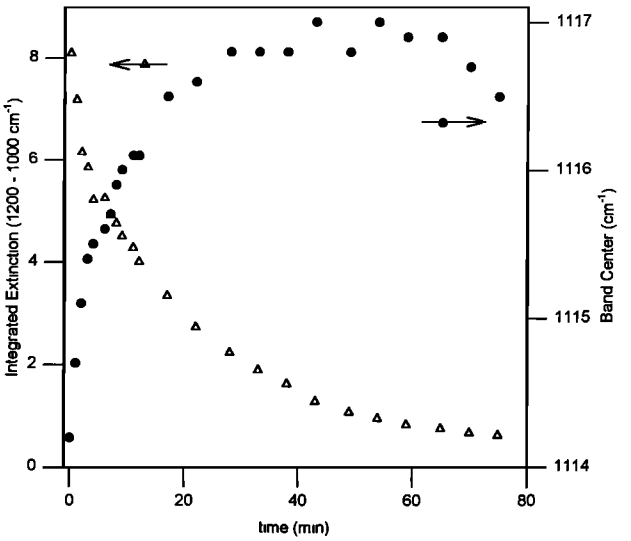

Figure 6. Results of a sedimentation experiment for an aerosol of initial average particle diameter of 0.3-μm. The open triangles represent the measured integrated extinction (1200 - 1000 cm^{-1}). The solid circles represent the wavenumber of the ν_3 (SO_4^{2-}) band center.

In a lognormal distribution the count median diameter, the count mode diameter, and count mean diameter are all numerically equivalent. These arithmetic averages correspond to the diameter that numerically has the largest value in a lognormal size distribution. In other applications, we will be interested in the mean (as opposed to median) volume of particles in a lognormal distribution. Here we are concerned with the volume, or equivalently the mass distribution within the aerosol.

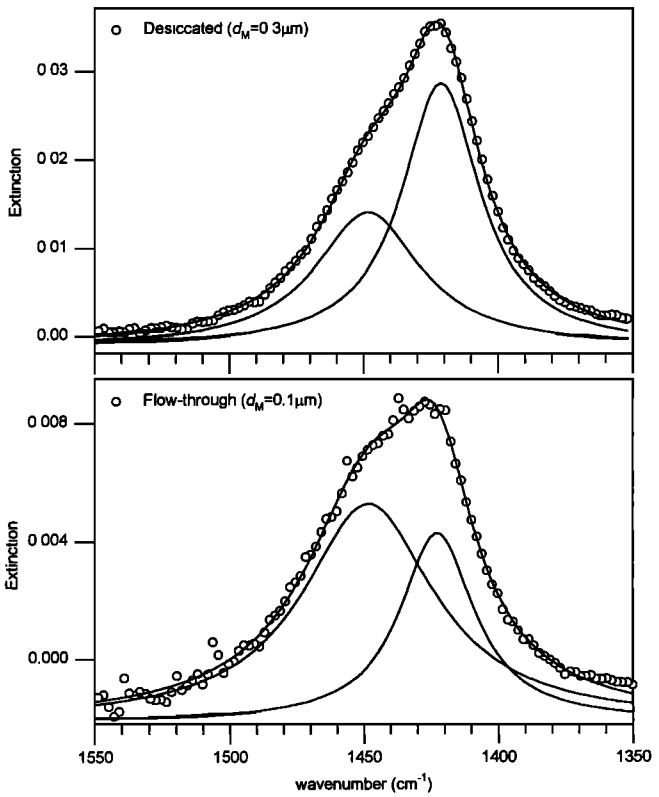

Figure 5. Extinction spectra from $\nu_4(NH_4^+)$ for desiccated 0.3-μm and flow-through 0.1-μm aerosols. The open circles represent the actual spectroscopically measured extinction values. The curves that follow the data points represent the fits obtained by combining the two lorentzian bands shown below the curves.

Spectroscopic absorption measurements, in the Rayleigh limit [*Bohren and Huffman*, 1983], respond in proportion to the volume of the particle (hence mass or number of molecules) in the aerosol. The average particle mass, $\overline{M}$, is defined as

$$\overline{M} = \frac{\sum_{i=1}^{J} M_i}{J} \tag{2}$$

where J is again the number of the particles and M_i is the mass of the ith particle. If the geometry of the particle is known, then $\overline{M}$ can be related to the particle size. Assuming nonporous spheres, the average mass is given by

$$\overline{M} = \frac{\pi}{6}\rho d_{\overline{M}}^{3} \tag{3}$$

where ρ is the density of the bulk material (1.77×10^3 kg m^{-3} for $(NH_4)_2SO_4$ [*Weast*, 1973]) and $d_{\overline{M}}$ is the diameter of average mass.

For a lognormal distribution, the Hatch-Choate equations can be used to convert one type of average to another [*Hinds*, 1982]. In particular,

$$d_{\overline{M}} = \bar{d}\exp\left(1.5 \ln^2 \zeta\right). \tag{4}$$

For the aerosols discussed in this paper, for which the ζ is 2.0, the right-hand side of (4) reduces to $(2.06)\bar{d}$. The average diameter used in this paper is the diameter of average mass, $d_{\overline{M}}$, unless otherwise specified.

Assuming that there is no change in the amount of $(NH_4)_2SO_4$ in each individual particle, it is possible to estimate the diameter of the completely dried particles (d_p) from that of the aqueous droplet (d_l) if we naively assume that desiccated

droplets form nonporous spheres of solid $(NH_4)_2SO_4$. (We shall examine this assumption later.) We then have

$$d_p = d_1 \sqrt[3]{10^3 \frac{c}{\rho}} \tag{5}$$

where c is the concentration of $(NH_4)_2SO_4$ in the droplet in kilograms per liter and the factor of 10^3 converts from kilograms per liter to kilograms per cubic meter. Equation (5) establishes a lower bound for the diameter of the aerosol. Using solution concentrations from 5.5×10^{-3} kg L^{-1} up to the saturation limit, (5) indicates that we have generated particles having average diameters, $d_{\bar{M}}$, from 0.1 to 0.5-μm.

Aerosol Photometry

The irradiance of light, I, passing through an aerosol is given by [*Bohren and Huffman*, 1983]

$$I = I_0 e^{-\alpha_{ext} z} \tag{6}$$

where I_0 is the incident irradiance, z is the path length (1 m for our cells), and α_{ext} is the extinction coefficient. (A condition for the validity of (6) is that multiple scattering effects of the aerosol are negligible. This condition is usually met for our samples as we shall see in calculations to follow.)

Light extinction by particles within the aerosol is a consequence of both absorption and scattering so that the extinction coefficient, α_{ext} (m^{-1}) can be resolved into

$$\alpha_{ext} = \alpha_{abs} + \alpha_{sca} \tag{7}$$

where α_{abs} is the absorption coefficient and α_{sca} the scattering coefficient. These coefficients can in turn be expressed as

$$\alpha_{ext}(d) = D_{part}(d) C_{ext}(d)$$
$$= D_{part}(d)[C_{abs}(d) + C_{sca}(d)] . \tag{8}$$

Here we have imagined the particles of the aerosol to be monodisperse spheres of diameter d. The particle cross sections $C(d)$ with appropriate subscripts have units (m^2 $particle^{-1}$) and the particle number density, $D_{part}(d)$, has units (particles m^{-3}). For some discussions it is helpful to refer to scattering or absorption efficiencies, $Q_{sca} = (4C_{sca})/(\pi d^2)$ or $Q_{abs} = (4C_{abs})/(\pi d^2)$, respectively, that are dimensionless cross sections having been normalized by the particle geometric cross sections. Later we shall extend the form of (8) to encompass particle distributions.

Since our spectroscopically experimentally measured ratio (T_b/T_s) is numerically equal to (I_0/I) we may rewrite extinction in terms of α_{ext}:

$$E \equiv \log_{10}\left(\frac{T_b}{T_s}\right) = \log_{10}\left(\frac{I_0}{I}\right) = \frac{\alpha_{ext} z}{2.303} . \tag{9}$$

Thus a spectroscopic measurement of E, together with a knowledge of $C_{ext}(d)$ and z can provide $D_{part}(d)$, the particle number density.

A method for calculation of $C_{abs}(d)$ and $C_{sca}(d)$ for spherical particles is given by Mie theory [*van de Hulst*, 1957; *Bohren and Huffman*, 1983; *Born and Wolf*, 1989]. The only physical parameter required (aside from d) is the complex index of refraction, $N = \eta + i\kappa$, of the bulk material of which the spherical particle is made. Fortunately, both the real index of refraction, η, and the imaginary index of refraction, κ, have been measured for crystalline $(NH_4)_2SO_4$ throughout the infrared region by *Toon et al.* [1976]. We have used the tabulated dispersion parameters for the c axis of the $(NH_4)_2SO_4$ crystal to obtain η and κ from 4000 to 600 cm^{-1}. For convenience these results are reproduced in Figure 7. (*Toon et al.* [1976] found, within experimental error, no differences in the complex indices of refraction among the three axes of the single crystal.)

As we shall see, both Q_{sca} and Q_{abs} vary considerably with particle diameter and wavenumber. We shall also find that for $d \leq 0.5$-μm, $Q_{sca} \ll Q_{abs}$ and in general the particle scattering cross section is small. These results follow from the Rayleigh limit criterion that qualitatively states that, for $\pi|m|d \ll \lambda$ ($m \equiv N/N_0$ where N_0 is the complex refractive index of the surrounding medium which in our experiments is air), particle scattering effects are small [*Bohren and Huffman*, 1983]. For our experiments with $d_{\bar{M}} \leq 0.5$-μm, wavelengths $\lambda \geq 2.5$-μm ($\leq$ 4000 cm^{-1}) and $|m| < 3$ (see Figure 7), the Rayleigh criterion is usually met. This will be demonstrated quantitatively in calculations to follow.

In exploring the effects of morphology and size on extinction, it is useful to normalize the cross section by the number of $(NH_4)_2SO_4$ molecules in the spherical particle or bulk crystalline sample. We shall call this the molecular cross section σ (m^2 $molecule^{-1}$). In the bulk crystalline sample we have $\alpha^{(bulk)} = 4\pi\kappa/\lambda$ from which the molecular (absorption) cross section $(NH_4)_2SO_4$ is obtained from

$$\sigma^{(bulk)} = \frac{4\pi(10^2)\kappa\tilde{\nu}}{p} \tag{10}$$

where $\tilde{\nu} = \lambda^{-1}$ and $p = 8.07 \times 10^{27}$ molecule m^{-3} is the molecular density of crystalline $(NH_4)_2SO_4$ [*Weast*, 1973]. (Since the units of $\tilde{\nu}$ are cm^{-1}, the factor of 10^2 provides SI units for $\sigma^{(bulk)}$.) The (extinction) cross section for a spherical particle of diameter d and volume $\pi d^3/6$ is calculated from

$$\sigma^{(sphere)} = \frac{6C_{ext}}{\pi p d^3} = \frac{3}{2}\frac{Q_{ext}}{pd} . \tag{11}$$

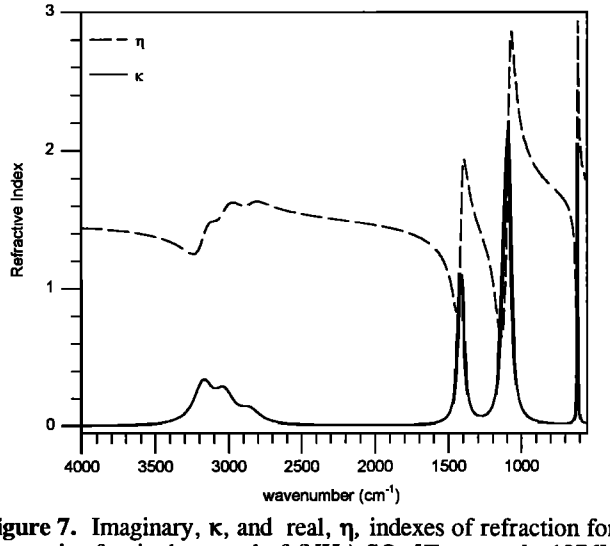

Figure 7. Imaginary, κ, and real, η, indexes of refraction for the c axis of a single crystal of $(NH_4)_2SO_4$ [*Toon et al.*, 1976].

We shall denote $\sigma^{(sphere)}$ at $\tilde{\nu}_0$ as $\sigma_0^{(sphere)}$.

As we shall see in the Mie theory calculations of Table 3, there is little change in band center and bandwidth for the $\nu_3(SO_4^{2-})$ mode of the spheres with variation in d from 0.1 to 0.5-μm. For larger spheres, d = 2.0-μm, for example, scattering dominates the extinction and the resultant spectrum differs significantly from that of the smaller spheres. Likewise, the cross section $\sigma_0^{(sphere)}$ and the integrated cross section

$$\bar{\sigma}^{(sphere)} = 10^2 \int_{band} \sigma^{(sphere)} d\tilde{\nu} \approx \frac{\pi}{2}(10^2)\, \sigma_0^{(sphere)} \Gamma \qquad (12)$$

change only slightly with d for small diameters. Integration over the band in (12) is approximated by the analytical result for a lorentzian profile with cross section maximum $\sigma_0^{(sphere)}$ and bandwidth Γ. Later we shall compare $\bar{\sigma}^{(sphere)}$ with

$$\bar{\sigma}^{(bulk)} = \frac{4\pi 10^4}{\rho} \int_{band} \kappa \tilde{\nu} d\tilde{\nu} \approx \frac{2\pi^2 (10^4) \kappa_0 \tilde{\nu}_0 \Gamma}{\rho} \qquad (13)$$

for the bulk sample. Again a lorentzian profile is assumed for the band integration with κ_0 the value of the imaginary index of refraction at the band center. (Since $\tilde{\nu}$ is given in wavenumber (cm^{-1}) the factor of 10^2 in (12) and 10^4 in (13) assures SI units for integrated cross section $\bar{\sigma}$ of meters per molecule.)

We shall find in Table 3 a (near) constancy of $\sigma_0^{(sphere)}$ for $d \leq 1.0$-μm of the $\nu_3(SO_4^{2-})$ mode. This result has an important application for photometric measurements. Using Beer's law [*Harrison et al.*, 1948] we have

$$E = \frac{D_{molec}\, \sigma^{(sphere)} z}{2.303} \qquad (14)$$

where D_{molec} is the average molecular density of $(NH_4)_2SO_4$ (molecule m^{-3}) in the aerosol sample. Given the value for $\sigma_0^{(sphere)}$, a spectroscopic measurement of the extinction at the band center, E_0, and the path length, z, we can determine D_{molec}.

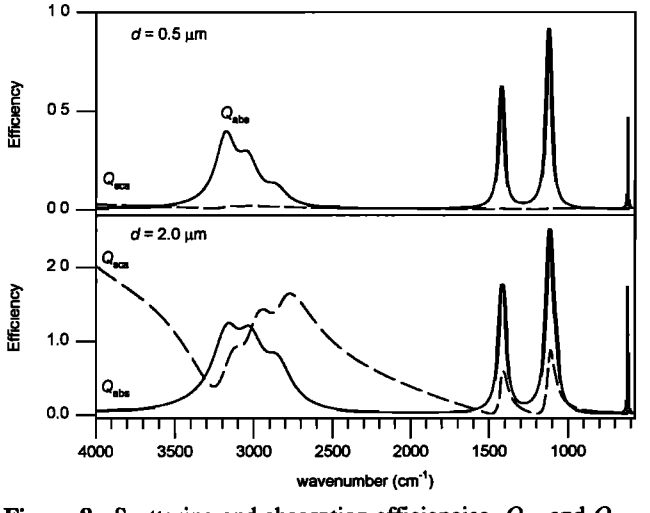

Figure 8. Scattering and absorption efficiencies, Q_{sca} and Q_{abs}, for d = 0.5-μm and d = 2.0-μm spheres of $(NH_4)_2SO_4$.

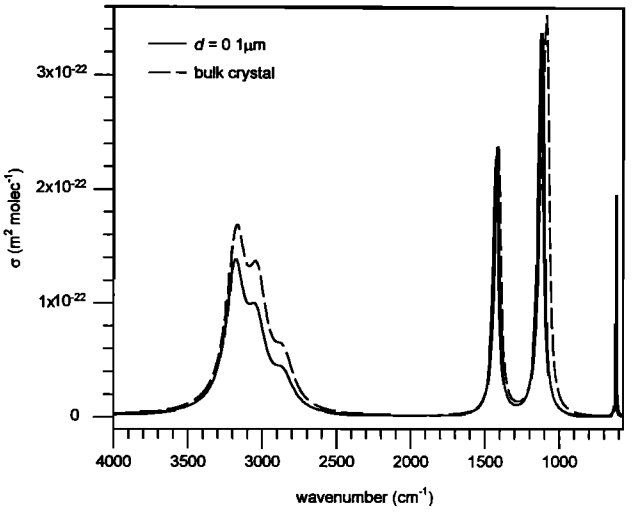

Figure 9. Calculated molecular cross sections for a d = 0.1-μm sphere and c axis crystal $(NH_4)_2SO_4$.

Mie Theory Calculations

Our Mie theory calculations of $Q_{abs}(d)$ and $Q_{sca}(d)$ were performed using the program BHMIE [*Bohren and Huffman*, 1983]. The optical constants used are those shown in Figure 7 [*Toon et al.*, 1976]. Our first calculations of $Q_{abs}(d)$ and $Q_{sca}(d)$ are for spheres of $(NH_4)_2SO_4$ of diameter d = 0.5-μm and 2.0-μm. These results are shown in Figure 8.

For 2.0-μm particles scattering dominates the extinction near 4000 cm^{-1} with an efficiency of 2, roughly 2 orders of magnitude larger than for d = 0.5-μm. In the region of $\nu_3(NH_4^+)$, absorption and scattering make comparable contributions. Since scattering maxima occur at lower wavenumbers than those of absorption, this will have the effect of red shifting the extinction band of $\nu_3(NH_4^+)$ for large particles. Scattering affects the region below 1500 cm^{-1} to a lesser extent. Nevertheless, the scattering contribution to $\nu_3(SO_4^{2-})$ will have the effect of lowering the extinction band center by several wavenumbers. This can explain the observed shifts in this feature for increased average diameters indicated in Tables 1 and 2. (Recall that a particle distribution with an average diameter of 0.5-μm will have contributions from larger sizes because of the wide size distribution.)

For 0.5-μm particles, scattering is negligible except at the highest wavenumbers. An analysis of the modes excited for spheres of this size shows that the lowest order mode, a_1, is dominant. Since this mode has a constant radial component of electric field throughout the sphere, it is called the mode of uniform polarization [*Bohren and Huffman*, 1983]. By contrast, higher order modes, b_1, a_2, etc., will make contributions to the excitations of the 2.0-μm particles particularly at shorter wavelengths.

The effect of morphology on the optical properties of $(NH_4)_2SO_4$ is illustrated in Figure 9. Here we compare molecular cross section of crystalline $(NH_4)_2SO_4$ in the bulk, $\sigma^{(bulk)}$, with $\sigma^{(sphere)}$ for a 0.1-μm sphere. The values of $\sigma^{(bulk)}$ were obtained using (10) and the complex index of refraction shown in Figure 7. The Mie calculations made use of (11). The spectroscopic signatures of the sphere do differ somewhat from those of bulk crystalline $(NH_4)_2SO_4$. This is particularly obvious in the roughly 30 cm^{-1} blue shift in the band center of $\nu_3(SO_4^{2-})$ of the sphere relative to the bulk. There is also an

Table 3. Calculation of $\nu_3(SO_4^{2-})$ Spectroscopic Constants For Spherical Crystals and BulkSingle Crystal $(NH_4)_2SO_4$

d, μm	ζ[a]	$\tilde{\nu}_0$, cm^{-1}	Γ, cm^{-1}	σ_0[b]	$\bar{\sigma}$[c]
0.1	1	1124.4	41.5	3.38	2.20
0.3	1	1124.2	41.6	3.39	2.21
0.5	1	1123.7	41.9	3.42	2.25
1.0	1	1121.6	44	3.5	2.4
2.0	1	1113.2	67	3.1	3.3
0.1	2.0	1124.1	43.1	3.39	2.29
0.5	2.0	1120.8	51	3.12	2.5
crystal	------	1092.5	62.9	3.53	3.49

[a] $\zeta = 1$ is for monodisperse particles. For $\zeta = 2.0$, the value given for d is the diameter of average mass ($d_{\bar{M}}$).
[b] In units of 10^{-22} m^2 $molecule^{-1}$.
[c] In units of 10^{-18} m $molecule^{-1}$.

overall attenuation of $\sigma^{(sphere)}$ relative to $\sigma^{(bulk)}$. However, qualitatively, the two curves follow each other rather closely.

A detailed comparison of the optical properties in the $\nu_3(SO_4^{2-})$ region for several monodisperse, $\zeta = 1$, sphere diameters and for the bulk crystal is presented in Table 3. Also listed are results for calculations over distributions of sphere diameters with $\zeta = 2.0$. Several interesting features are revealed by the series of calculations. First, $\tilde{\nu}_0$ shifts to lower frequency and Γ becomes larger as the particle diameter increases. For $d \leq 1.0$-μm, $\sigma_0^{(sphere)}$ and $\bar{\sigma}^{(sphere)}$ increase only slightly with increasing diameter. The constancy (within 10%) is expected for spheres within the Rayleigh limit since, for this case, $C_{abs}(d)$, the particle cross section, is proportional to volume (i.e,. the number of $(NH_2)_4SO_4$ molecules) and because $C_{abs} \gg C_{sca}$, hence $C_{ext} \approx C_{abs}$ [*Bohren and Huffman*, 1983]. The abrupt red shift in $\tilde{\nu}_0$ and increase of Γ from $d = 1.0$-μm to $d = 2.0$-μm occurs because scattering, which achieves its maximum at lower frequency, contributes significantly to the extinction by the larger particle. This is apparent in Figure 8. Scattering is also responsible for the sudden increase in $\bar{\sigma}^{(sphere)}$ for $d = 2.0$-μm. Since the optical response of single crystal and spherical particles, are expected to be different because of their morphologies, variations of $\tilde{\nu}_0$, Γ, σ_0, and $\bar{\sigma}$ in Table 3 are not surprising.

We now use (14) to determine D_{molec} in the 0.5-μm flow-through spectrum. The extinction at the band center of $\nu_3(SO_4^{2-})$ is 1.1 from Figure 3. Using $\sigma_0^{(sphere)} = 3.1 \times 10^{-22}$ m^2 $molecules^{-1}$ gives $D_{molec} = 7.9 \times 10^{21}$ molecules m^{-3}. By assuming that the particles are non-porous spheres with $d_{\bar{M}} = 0.5$-μm, each particle contains, on average 5.3×10^8 molecules. Dividing D_{molec} by the average number of molecules per particle gives $D_{part} = 1.5 \times 10^{13}$ particles m^{-3}. This is roughly an order of magnitude smaller than the rated value of the atomizer. However, losses of particles to the walls and transfer tubing of the aerosol generation system are expected. These calculations for spherical particles show that, in the Rayleigh limit, the extinction contains information on the number of $(NH_4)_2SO_4$ molecules whereas the wavenumber location of the band center and the band shape contains information on the particle size.

Since our experiments with aerosols and aerosols in the atmosphere contain a polydisperse distribution of particles, we must now deal with this condition in understanding their spectroscopy. The fraction of particles having diameters between $\ln(d)$ and $\ln(d) + d(\ln d)$, df, is given by the lognormal frequency function [*Hinds*, 1982]

$$df = \frac{1}{\sqrt{2\pi}\ln\zeta}\exp\left[-\frac{(\ln d - \ln\bar{d})^2}{2(\ln\zeta)^2}\right]d(\ln d) \quad (15)$$

This frequency function may be approximated numerically in the following manner. In a log-normal distribution, more than 99.9% of the particles will have diameters between $\bar{d}\zeta^{-5}$ and $\bar{d}\zeta^{5}$. Let ℓ represent this range

$$\ell \equiv \ln(\bar{d}\zeta^{5}) - \ln(\bar{d}\zeta^{-5}) \quad (16)$$

The lognormal frequency function can be partitioned into L channels of equal width in logspace, where L is the integer closest to $S\ell$ and S is an arbitrary positive integer chosen to give the desired number of channels in the particle distribution. When the channels are labeled $i = 0, 1, 2, \ldots, L$, the diameter of particles in the ith channel is given by

$$\ln(d_i) = \ln(d\zeta^{-5}) + \frac{i}{25} \quad \text{or} \quad d_i = d\zeta^{-5}\left[\exp\left(\frac{i}{25}\right)\right] \quad (17)$$

The numerical approximation of the frequency function is then

$$\Delta f_i = \frac{1}{\sqrt{2\pi}\ln\zeta}\exp\left[-\frac{(\ln d_i - \ln\bar{d})^2}{2(\ln\zeta)^2}\right]\frac{\ell}{L} \quad (18)$$

Thus the cross section (with the appropriate subscript) for a lognormal distribution of diameters is given by

$$\sigma^{(sphere)} = \sum_{i=0}^{L}\frac{\Delta f_i Q(d_i) d_i^2}{d_{\bar{M}}^3 \rho} \quad (19)$$

Using (19) (with $S=100$), we have calculated $\sigma_0^{(sphere)}$ and using (12), $\bar{\sigma}^{(sphere)}$ for $d_{\bar{M}} = 0.1$-μm and 0.5-μm, both with $\zeta = 2.0$. These results are listed in Table 3. Decreasing the channel width by increasing S to 1000 changes $\sigma_0^{(sphere)}$ and $\bar{\sigma}_0^{(sphere)}$ by less than 0.1% showing that we have covergence of the calculated spectroscopic properties.

We have attempted to match an experimental spectrum with that obtained from Mie theory by using the following equation.

$$\alpha_{ext} = \frac{1}{4}\sum_{i=0}^{L}\Delta f_i D_{part}\left[Q_{sca}(d_i) + Q_{abs}(d_i)\right]\pi d_i^2 \quad (20)$$

Equation (20) is then substituted into (14) to obtain an extinction spectrum. Figure 10 shows such a calculated spectrum obtained using $d_{\bar{M}} = 0.5$-μm, $\zeta = 2.0$, and $D_{part} = 1.5 \times 10^{13}$ particles m^{-3} compared with the 0.5-μm flow-through spectrum from Figure 3.

The agreement between the calculated and observed spectra is reasonable on many counts. The calculated scattering contribution between 1500 and 2500 cm^{-1} and above 3500 cm^{-1} is in good agreement with the experi-mental spectrum. The positions of the $\nu_3(NH_4^+)$, $\nu_4(NH_4^+)$, and $\nu_4(SO_4^{2-})$ band centers are within 1%. However, while extinction values for $\nu_3(SO_4^{2-})$ in the two spectra match, the calculation overestimates the extinctions for $\nu_4(NH_4^+)$ and $\nu_4(SO_4^{2-})$. The overestimation in the $\nu_4(NH_4^+)$ band may be due in part to the

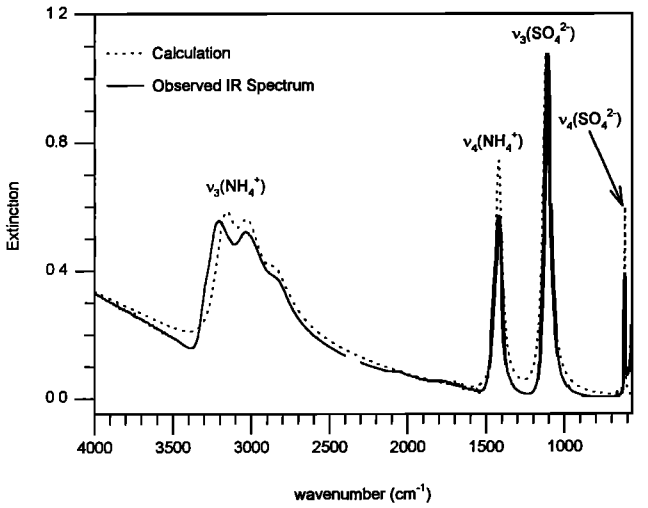

Figure 10. Spectrum of the flow-through aerosol with $d_{\bar{M}}$ = 0.5-μm from Figure 3 compared with the results of a Mie calculation using $D_{part} = 1.5 \times 10^{13}$ m^{-3}, z = 1 m, $d_{\bar{M}}$ = 0.5-μm, and ζ = 2.0.

measured optical constants in this region. The data of Toon et al. suggest a singlet in this region, while the experimental feature is clearly a doublet which is wider than the singlet. Thus band broadening can result in extinction reduction at the band center without a necessary change in integrated extinction for a band. (We shall explore this phenomenon below.) A similar broadening of the $\nu_4(SO_4^{2-})$ band in the aerosol particles could likewise account for the discrepancies in this spectral region of Figure 10. The differences in the $\nu_3(NH_4^+)$ region are more severe. The high-frequency shoulder near 3300 cm^{-1} in the observed spectrum is absent in the Mie calculation. Finally, the scattering contribution in the calculation, apparent above 3500 cm^{-1}, in the region above 1500 cm^{-1}, and into the $\nu_3(NH_4^+)$ absorption is slightly overestimated in the Mie calculation.

We now examine the frequency differences in the $\nu_3(SO_4^{2-})$ band centers more closely. Comparisons of Tables 1 and 3 show a discrepancy of 10 cm^{-1} between the measured frequency and both polydisperse calculations. Since the calculated frequencies differ by only 3.3 cm^{-1} between $d_{\bar{M}}$ = 0.1-μm and $d_{\bar{M}}$ = 0.5-μm, further reasonable changes in diameter will not bring the calculated and observed peaks into agreement. While Mie theory is appropriate for aerosols containing droplets (since they are spheres), its application to nonspherical particles may be inappropriate. The scanning electron microscope photographs [*Perry et al.*, 1978] revealed $(NH_4)_2SO_4$ particles spherical in shape. However, the aerosol droplets, initially produced, were desiccated in a furnace at 210°C before microscopic examination. Under these conditions $(NH_4)_2SO_4$ is known to decompose producing $(NH_4)HSO_4$ which in turn can melt [*Kroschwitz*, 1992]. Thus while the furnace-treated sulfate particles were spherical, our aerosols, desiccated under ambient conditions, may well contain nonspherical crystals. Disagreements we find in the Mie calculation in Figure 10 with the observed aerosol spectrum for other modes may also be a consequence of morphology differences: the calculation was for spheres but the experiment may have contained nonspherical crystals. Although the particles may not be spherical, Mie theory is a valid first approximation for the value of extinction by the vibrational modes of the molecules.

As we shall show later, we believe the 0.5-μm flow-through aerosol contains crystals (as opposed to droplets), generated over a seconds timescale, which may not be well ordered. This lack of homogeneity may be responsible for bandwidth increases of some of the features. By contrast, the crystals from which the optical constants are taken were carefully grown over a 1 year period [*Toon et al.*, 1976] and are likely to yield the most narrow absorption features. Thus the extinction discrepancies in Figure 10 may be merely a consequence of crystal inhomogeneities. Considering the vastly different methods of $(NH_4)_2SO_4$ sample preparation, the agreements in Figure 10 should probably be considered remarkable and another testimony to Mie theory.

The condition that multiple scattering is unimportant to the aerosol spectroscopy and that (6) is valid is that $\alpha_{ext} z \ll 1$ [*Bohren and Huffman*, 1983]. Using (9), this condition is equivalent to $E \ll 1$. The scattering contribution to extinction at lower wavenumbers, < 2000 cm^{-1}, is seen from Figure 10 to be < 0.1. So multiple scattering is unimportant in this region. However, toward 4000 cm^{-1} where $E \approx 0.3$ multiple scattering may affect the spectroscopy and could contribute to the discrepancy between the calculated and observed spectra.

Sedimentation and Coagulation

The sedimentation velocity of a small sphere is given by the Stokes equation with the slip correction factor [*Hinds*, 1982]:

$$v(d) = \frac{\rho d^2 g}{18\gamma}\left(1 + \frac{l}{d}\left[2.514 + 0.800\exp\left(-0.55\frac{l}{d}\right)\right]\right) \quad (21)$$

where g is the gravitational acceleration constant (9.81 m s^{-2}), γ is the viscosity of air at 20°C and 1 bar total pressure (1.81 $\times$ 10^{-5} Pa s [*Hinds*, 1982]), and l is the average mean free path of gas molecules in air under the same conditions (6.6 $\times$ 10^{-8} m [*Hinds*, 1982]). The observed extinction half-life for the particle sedimentation process shown in Figure 6 is approximately 11 min. If the particles were monodisperse, this half-life would correspond to the time required for a particle to fall half the diameter of the cell. Since the inside diameter of cell is about 40 mm, this leads to a sedimentation velocity of 3.0×10^{-5} m s^{-1}. Solving (21) for d leads to an estimated diameter of 0.7-μm, a factor of 2 larger than that predicted by (5). The problem with estimating the diameter from such a simplistic analysis of the sedimentation behavior is that the observed extinction decay is weighted by the lognormal frequency function and the extinction depends roughly on the diameter cubed. This implies that the large particles dominate the extinction spectrum only at early times since they settle. Also, the sedimentation velocities in these size distributions range over 2 to 3 orders of magnitude. This approach also overlooks aerosol coagulation.

Although these aerosols have fairly high numerical particle densities, the collision rate is not very large. The rate of collision in an aerosol containing monodisperse particles with any specific particle is $8\pi d\beta D_{part}$, where β is the particle diffusion coefficient [*Hinds*, 1982]. Taking $D_{part} = 5 \times 10^{13}$ m^{-3}, d=0.3-μm, and $\beta = 5 \times 10^{-12}$ m^2 s^{-1} [*Hinds*, 1982] gives 0.002 s^{-1}. The reciprocal of this quantity is the time between collisions, 500 s. This time, about 8 min, is thus comparable to the time that characterizes sedimentation. Thus coagulation and sedimentation are occurring simultaneously.

The +3 cm^{-1} shift observed for $\nu_3(SO_4^{2-})$ during sedimentation is consistent with the +3.3 cm^{-1} shift shown in Table 3 which was calculated for the polydisperse particles when $d_{\overline{M}}$ varies from 0.5-μm to 0.1-μm. Thus the observed spectroscopic changes during particle sedimentation and coagulation are complex and only partially understood.

Particle Morphology and Composition

In this section we explore the infrared spectroscopic signature of liquid water in the $(NH_4)_2SO_4$ aerosol spectra. We also identify characteristic features that can allow one to distinguish between supersaturated solution and crystalline $(NH_4)_2SO_4$ aerosols.

Figure 4 shows IR spectra of a near-saturated (0.64 kg L^{-1}) aqueous solution of $(NH_4)_2SO_4$ [*Remsberg*, 1971], the 0.3-μm flow-through aerosol, and the desiccated 0.3-μm aerosol. The shoulder near 3400 cm^{-1} in the aqueous solution is assigned to the ν_1, ν_3 stretching vibrations of liquid water and a feature near 1650 cm^{-1} is associated with the ν_2 bending vibration [*Downing et al.*, 1977]. The relatively weaker feature near 3450 cm^{-1} in the 0.3-μm flow-through aerosol spectrum and its companion near 1650 cm^{-1} are likewise assigned to water extinctions as indicated in Table 2. As expected, the ν_1, ν_2, and ν_3 extinctions that are the infrared signatures for liquid water [*Downing and Williams*, 1975] are missing in the desiccated aerosol spectrum (see Figures 2 and 4 and Table 1). Since the 0.3-μm flow-through aerosol contains water, we are led to two possible conclusions: the aerosol contains particles composed of both crystalline $(NH_4)_2SO_4$ and adsorbed water or that the aerosol contains supersaturated aqueous $(NH_4)_2SO_4$ droplets.

If the feature at 3450 cm^{-1} were due to water adsorbed onto the surface of the particles, then the spectroscopic response would be proportional to the surface area of the particles. Thus the extinction of adsorbed features relative to bulk features should decrease as the ratio of surface to volume decreases. This is not evident in Figure 3. The height of the 3450 cm^{-1} relative to the other features in the spectrum is the same for both the 0.1-μm and 0.3-μm spectra. We conclude then that it is unlikely that the aerosol consists of both crystalline and saturated aqueous solution $(NH_4)_2SO_4$.

Consider now the possibility of supersaturated droplets. Tang et al. [1995] have reported that single $(NH_4)_2SO_4$ microparticles that have deliquesced at 81% RH will remain supersaturated until the relative humidity falls below 37%, at which point the droplet recrystallizes. This solution can thus supersaturate to an H_2O-to-$(NH_4)_2SO_4$ molecular ratio of approximately 2.5 [*Tang et al.*, 1995]. The ratio of H_2O-to-$(NH_4)_2SO_4$ in the near-saturated solution shown in Figure 4 is approximately 11. The feature at 3450 cm^{-1} may be used to estimate the amount of liquid water in an aerosol if we assume that the peak extinction is proportional to the number of water molecules. Comparing the 3450 cm^{-1} band extinction in the aqueous spectrum to that in the flow-through spectrum, there appears to be about 3 times as much water in the aqueous solution spectrum as in the flow-through aerosol spectrum. This gives an H_2O-to-$(NH_4)_2SO_4$ ratio of about 3 in the flow-through spectrum, which is comparable to the supersaturated solutions observed by Tang et al. [1995] in the 30±5% RH range. We conclude then that the 0.3-μm flow-through aerosol of Figures 3 and 4 consist of supersaturated droplets. Since relative extinction of the 3450 cm^{-1} feature for the 0.1-μm flow-through aerosol in Figure 3 is comparable to that of the 0.3-μm sample, it too must consist of supersaturated droplets and at essentially the same concentration.

Since the particles are in the cell for only a few seconds during the flow-through experiments (as opposed to the ~8 min interval between collisions calculated in the previous section), it is unlikely that these particles could collide with each other and crystallize, so the comparison with the isolated microparticle of Tang et al. is valid. Furthermore, metastable liquid aerosols have been found to be ubiquitous even in natural environments [*Rood et al.*, 1989], where there is ample time for crystallization.

The flow-through spectra shown in Figure 3 demonstrate behavior that is similar to that of the desiccated aerosols: as the average diameter increases, the $\nu_3(SO_4^{2-})$ and $\nu_4(SO_4^{2-})$ bands and the $\nu_3(NH_4^+)$ shift to lower wavenumbers and broaden. The notable exception is $\nu_3(SO_4^{2-})$ for the 0.5-μm flow-through aerosol which is narrower than the band in the 0.1- and 0.3-μm desiccated aerosols. In addition, there is no shoulder at 3450 cm^{-1} in the 0.5-μm flow-through spectrum and the diffuse feature at 1650 cm^{-1} is missing. This suggests that this spectrum is not of supersaturated $(NH_4)_2SO_4$, but rather of crystalline $(NH_4)_2SO_4$. Since the aqueous solution that was used to generate these particles was saturated to begin with, the conditions in these droplets favor crystallization.

Figure 5 shows the resolution of the two overlapping features of $\nu_4(NH_4^+)$ for the desiccated $d_{\overline{M}}$ = 0.3-μm (crystalline) and the flow-through $d_{\overline{M}}$ = 0.1-μm (supersaturated droplet). While the peak centers and bandwidths of the two deconvoluted features are the same in both spectra, the relative extinctions (and hence the overall band shape) are different. This difference in relative extinctions was evident in all aerosols believed to contain crystalline or supersaturated droplet particles. Thus the $\nu_4(NH_4^+)$ region can also be used to distinguish crystalline from supersaturated $(NH_4)_2SO_4$ particles.

The $\nu_3(SO_4^{2-})$ region is also sensitive to the presence of water. In the spectra of desiccated aerosols, the band is a symmetric singlet, while in the spectra of flow-through aerosols the band is asymmetric with a trailing edge toward low wavenumbers.

Yet another spectroscopic signature that can distinguish between the crystalline particles and the metastable droplets is

Table 4. Comparison of Peak Extinction, E_0, and Integrated Extinction, $\overline{E}$, Ratios of $\nu_3(SO_4^{2-})$ to $\nu_4(NH_4^+)$ for $(NH_4)_2SO_4$

$d_{\overline{M}}$, μm	ζ	Type	$\frac{E_0(\nu_3)}{E_0(\nu_4)}$	$\frac{\overline{E}(\nu_3)}{\overline{E}(\nu_4)}$
---	---	aqueous[a]	2.8	2.6
0.1	~2	flow-through	2.7	1.5
0.3	~2	flow-through	2.4	1.8
0.5	~2	flow-through	1.9	1.6
0.2	~2	desiccated	2.1	1.4
0.3	~2	desiccated	1.9	1.5
0.5	~2	desiccated	1.9	1.5
0.5	2.0	calculated	1.4	1.3
---	---	single crystal[b]	1.4	1.8

[a]3.2 *M* [*Downing et al.*, 1977].
[b]From Toon et al. [1976].

the ratio of the peak extinction, E_0, of $\nu_3(SO_4^{2-})$ to $\nu_4(NH_4^+)$ listed in Table 4. Also listed are the peak extinction ratio for the calculated spectrum shown in Figure 10, and the ratios of $\kappa_0\tilde{\nu}_0$ (which is proportional to α_{abs}) for bulk crystalline $(NH_4)_2SO_4$ [*Toon et al.*, 1976], and bulk 3.2 *M* $(NH_4)_2SO_4$ [*Downing et al.*, 1977]. Table 4 shows that the ratio decreases as a function of size for the flow-through aerosol, perhaps due to increasing $(NH_4)_2SO_4$ concentration. The smallest particles, 0.1-μm, have a ratio of 2.7 which is close to that of the bulk aqueous solution value of 2.8. While at the other extreme, the 0.5-μm flow-through ratio of 1.9 agrees very well with the desiccated ratios which are 2.0 ± 0.1. However, even the desiccated ratios are not close to that observed for the crystalline phase or in the calculated spectrum. Table 4 also lists the ratio of $\bar{E}$ (the extinction integrated over the band) of $\nu_3(SO_4^{2-})$ to $\nu_4(NH_4^+)$. With the exception of the bulk 3.2 M $(NH_4)_2SO_4$, these values are constant within experimental uncertainty. Thus the observed change in the ratios of peak extinction are not caused by changes in the oscillator strengths of the modes, but rather are due to changes in the widths of the features.

Proposed Field Experiment

While the first field infrared measurement of stratospheric ice particles has just been reported [*Toon and Tolbert*, 1995], we know of no in situ tropospheric aerosol infrared extinction spectroscopy. We propose an experiment to spectroscopically explore sulfate in arctic haze.

In the spring (March or April), a faint white haze is often visible in the arctic troposphere. This haze, rich in sulfates of anthropogenic origin, forms a band a few kilometers thick that can cover an area as large as the African continent and may have a profound effect on the polar climate [*Shaw et al.*, 1993]. While the chemical composition of the collected haze particles has been measured a number of times [*Shaw and Khalil*, 1989] their in situ structure is unknown and is likely to be affected by the collection process. Our proposed experiment will take place using an airborne FT-IR directed toward the Sun as the source radiation. Flights would take place north of the arctic circle.

The spectroscopic feature most promising for detection is that of $\nu_3(SO_4^{2-})$ which is fortunately in the 10-μm (1000 cm^{-1}) atmospheric window [*Wayne*, 1991]. The extinction by this sulfate feature (or nearby HSO_4^- or H_2SO_4 [*Anthony et al.*, 1995]) will be significant under the conditions of the proposed experiment as the following feasibility calculation shows. A typical mass concentration of SO_4^{2-} (as $(NH_4)_2SO_4$, $NH_4(HSO_4)$, H_2SO_4, etc.) in the haze is 1-$\mu g\ m^{-3}$ [*Shaw and Khalil*, 1989] that corresponds to a molecular sulfate density of $D_{molec} = 5 \times 10^{15}\ m^{-3}$. The effective path length looking edge on into the haze layer toward the Sun near the horizon might be $z = 50$ km. Using the sulfate molecular optical cross section of $\sigma_0^{(sphere)} = 3.4 \times 10^{-22}\ m^2\ molecule^{-1}$ (see Table 3) and (14), we arrive at an extinction due to absorption of $E = 4 \times 10^{-2}$. Extinction due to scattering in the visible region will make the arctic haze, looking into it edge on, nearly opaque. However, total scattering in the $\nu_3(SO_4^{2-})$ region (including contributions from particles other than sulfates) will be small based on extinction estimations [*Shaw et al.*, 1993]. The extinction level, if set by noise from the FT-IR would be 5×10^{-4} (e.g., see Figure 2). Thus the signal to noise for the field experiment, if limited by the spectrometer, would be $\sim 10^2$. Other contributions to noise, such as atmospheric fluctuations, will lower this figure of merit. (The signal to noise level in the study of polar stratospheric cloud particles, which has proved useful in characterizing the ice composition, appears to be ~2 [*Toon and Tolbert*, 1995].)

There are a number of reasons for proposing the arctic for an initial aerosol field experiment. First the remote polar environment is relatively clean except for the arctic haze to be studied. Spectroscopic interference by water vapor, the strongest infrared atmospheric absorber, is reduced since its pressure at a typical arctic March temperature of −25°C is 2 orders of magnitude lower than at 25°C [*Warneck*, 1988].

What might one hope to learn from the arctic experiment? First a successful measurement would demonstrate that in situ infrared spectroscopy of tropospheric aerosols is possible. Along the way one would uncover the practical difficulties in field spectroscopy and (hopefully) how to alleviate them. Second, it should be possible to determine the composition of the aerosol. There are several features that can be used to distinguish between the particle as crystalline or as supersaturated droplet as we have shown. Moreover, the change in the profile of $\nu_4(NH_4^+)$ and the presence of the shoulder near 3450 cm^{-1} in $\nu_3(NH_4^+)$ can serve as qualitative indicators of the presence of aqueous $(NH_4)_2SO_4$. It may be possible to use the ratio of band heights or band areas in $\nu_4(NH_4^+)$ to determine the H_2O-to-$(NH_4)_2SO_4$ ratio. Unfortunately, the $\nu_3(SO_4^{2-})$ region appears to be only slightly sensitive to the phase. However, the singlet nature of this band is quite easily distinguished from the triplet observed for liquid H_2SO_4 films [*Anthony et al.*, 1995], so this region may be useful to determine sulfate type. Although there are measurable bands shifts of the spectrum of one particle with respect to another which are size dependent, particularly in $\nu_3(SO_4^{2-})$ where the band center can be located with good precision, these shifts are small and it is unlikely that they will be useful in determining particle size.

Conclusion

We have presented infrared extinction spectra of suspended $(NH_4)_2SO_4$ particles over a broad spectral range. A metastable aerosol composed of a supersaturated aqueous $(NH_4)_2SO_4$ droplets has been observed as has an aerosol containing crystalline particles. We have shown that spectroscopic signatures of $(NH_4)_2SO_4$ aerosols can be analyzed to obtain information about the water content of the particles. The extinction spectra of $(NH_4)_2SO_4$ particles which are small with respect to the wavelength of light are somewhat different than those predicted by Mie theory. Some of the deviations from bulk properties can be explained qualitatively by Mie theory. A quantitative understanding of the optical properties requires detailed information about the size and shape of the particles, which is unavailable. Finally, we have presented a simple calculation which suggests that infrared spectroscopic field measurements of sulfate aerosols are feasible.

Appendix

Three different types of curve-fitting routines were used in this study to determine the band positions and bandwidths. In all cases, the parameters were optimized using the nonlinear least squares fit routine in Sigma Plot (Jandel Scientific). All uncertainties reported in Tables 1 and 2 are twice the standard error computed by the nonlinear least squares program.

Band centers for $\nu_3(SO_4^{2-})$ and $\nu_4(SO_4^{2-})$ were deter-mined by fitting a parabola to the points near the band maximum. The parabolic equation was

$$E(\tilde{\nu}) = -k\left(\tilde{\nu} - \tilde{\nu}_0\right)^2 + E_0 \quad \text{(A1)}$$

where k, $\tilde{\nu}_0$, and E_0 were adjustable parameters corres-ponding to the width, band center, and extinction at the band center, respectively. A computer routine was employed that determined the extinction difference between the baseline and the band maximum. All points that had extinction differences which were greater than or equal to a fraction of the peak extinction difference were used in the least squares fit. These fractions are listed in the footnotes of Tables 1 and 2.

A single lorentzian band was fit to $\nu_3(SO_4^{2-})$ and $\nu_4(SO_4^{2-})$ to determine the full width at half maximum. The lorentzian equation was

$$E(\tilde{\nu}) = \frac{h}{1 + 4\left(\dfrac{\tilde{\nu} - \tilde{\nu}_0}{\Gamma}\right)^2} + c \quad \text{(A2)}$$

where h, Γ and c were adjustable parameters corresponding to the extinction, band center, full width at half maximum, and baseline, respectively. All points between 1200 and 1000 cm^{-1} were used in the least squares fit.

For $\nu_4(NH_4^+)$, a pair of lorentzian profiles were fit to the experimental data. The fitting equation was

$$E(\tilde{\nu}) = \frac{h_1}{1 + 4\left(\dfrac{\tilde{\nu} - \tilde{\nu}_1}{\Gamma_1}\right)^2} + \frac{h_2}{1 + 4\left(\dfrac{\tilde{\nu} - \tilde{\nu}_2}{\Gamma_2}\right)^2} + c \quad \text{(A3)}$$

where h_1, h_2, Γ_1, Γ_2, $\tilde{\nu}_1$, $\tilde{\nu}_2$, and c are adjustable parameters corresponding to the extinctions, full widths at half maximum, band centers, and the baseline of two lorentzian curves. All points between 1550 and 1350 cm^{-1} were used in the least squares fit. A similar procedure with four sets of parameters was used to determine the band centers for $\nu_3(NH_4^+)$.

Acknowledgments. Funding for this research was provided by a grant from the National Science Foundation (ATM93-03058). David Regan constructed the desiccating cell. We would like to thank Ignatius Tang for providing us with a preprint of his paper and Robert Disselkamp and Braig Bohren for helpful discussions. We are particularly grateful to the reviewers for their detailed constructive criticisms of the drafts of this paper.

References

Abbatt, J. P. D., and M. J. Molina, Heterogenous interactions of $ClONO_2$ and HCl on nitric acid trihydrate at 202 K, *J. Phys. Chem., 96,* 7674, 1992.

Anthony, S. E., R. T. Tisdale, R. S. Disselkamp, and M. A. Tolbert, FTIR studies of low temperature sulfuric acid aerosols, *Geophys. Res. Lett., 22,* 1105, 1995.

Bohren, C. F., and D. R. Huffman, *Absorption and Scattering of Light by Small Particles,* 530 pp.,Wiley-Interscience, New York, 1983.

Born, M., and E. Wolf, *Principles of Optics*, 6th ed., 808 pp., Pergamon, Tarrytown, N.Y., 1989.

Charlson, R. J., S. E. Schwartz, J. M. Hales, R. D. Cess, J. A. Coakley Jr., J. E. Hansen, and D. J. Hofmann, Climate forcing by anthropogenic aerosols, *Science, 255,* 423, 1992.

Downing, H. D., L. W. Pinkley, P. P. Sethna, and D. Williams, Optical constants of ammonium sulfate in the infrared, *J. Opt. Soc. Am., 67,* 186, 1977.

Downing, H. E. and D. Williams, Optical constants of water in the infrared, *J. Geophys. Res., 80,* 1656, 1975.

Hanson, D. R., and A. R. Ravishankara, Reaction of $ClONO_2$ with HCl on NAT, NAD, and frozen sulfuric acid and hydrolysis of N_2O_5 and $ClONO_2$ on frozen sulfuric acid, *J. Geophys. Res., 98,* 22931, 1993.

Harrison, G. R., R. C. Lord, and J. R. Loofbowrow, 605 pp., *Practical Spectroscopy*, Prentice-Hall, Englewood Cliffs, N. J. 1948.

Hinds, W. C., *Aerosol Technology: Properties, Behavior, and Measurement of Airborne Particles*, 424 pp., Wiley-Interscience, New York, 1982.

Johnson, S. A., and R. Kumar, Composition and spectral characteristics of ambient aerosol at Mauna Loa Observatory, *J. Geophys. Res., 96,* 5379, 1991.

Kroschwitz, J. I., (Ed.), *Kirk-Othmer Encyclopedia of Chemical Technology*, 4th ed., vol. 2, 706 pp., Wiley-Interscience, New York, 1992.

Mudd, H. T., Jr., C. H. Kruger, and E. R. Murray, Measurement of IR laser backscatter spectra from sulfuric acid and ammonium sulfate aerosols, *Appl. Opt., 21,* 1146, 1982.

Perry, R. J., A. J. Hunt, and D. R. Huffman, Experimental determinations of Mueller scattering matrices for nonspherical particles, *Appl. Opt., 17,* 2700, 1978.

Remsberg, E. E., Radiative properties of several probable constituents of the atmospheric aerosols, Ph.D. thesis, Univ. of Wis., Madison, June 1971.

Rood, M. J., M. A. Shaw, T. V. Larson, and D. S. Covert, Ubiquitous nature of ambient metastable aerosol, *Nature, 337,* 537, 1989.

Schroeder, W. H., and P. Urone, Formation of nitrosyl chloride from salt particles in air, *Environ. Sci. Technol., 8,* 756, 1974.

Shaw, G. E. and M. A. K. Khalil, Arctic haze, in *The Handbook of Environmental Chemistry*, O. Hutzinger (Ed.), vol. 4B, pp. 70-111, Springer-Verlag, New York, 1989.

Shaw, G. E., K. Stammes, and Y. X. Hu, Arctic haze: Perturbation to the radiation field, *Meteorol. Atmos. Phys., 51,* 227, 1993.

Tang, I. N., K. H. Fung, D. G. Imre, and H. R. Munkelwitz, Phase transformation and metastability of hygroscopic microparticles, *Aerosol Sci. Technol, 23,* 443, 1995.

Tolbert, M., Sulfate aerosol and polar stratospheric cloud formation, *Science, 264,* 527, 1994.

Toon, O. B. and M. Tolbert, Spectroscopic evidence against nitric acid trihydrate in polar stratospheric clouds, *Nature, 375,* 281, 1995.

Toon, O. B., J. B. Pollack, and B. N. Khare, The optical constants of several atmospheric aerosol species: Ammonium sulfate, aluminum oxide, and sodium chloride, *J. Geophys. Res., 81,* 5733, 1976.

van de Hulst, H. C., *Light Scattering by Small Particles*, 470 pp., John Wiely & Sons, New York, 1957.

Vogt, R., and B. J. Finlayson-Pitts, A diffuse reflectance infrared Fourier transform spectroscopic (DRIFTS) study of the surface reaction of NaCl with gaseous NO_2 and HNO_3, *J. Phys. Chem., 98,* 3747, 1994.

Warneck, P., *Chemistry of the Natural Atmosphere*, 757 pp., Academic, San Diego, Calif. 1988.

Wayne, R.P., *Chemistry of Atmospheres*, 2nd ed., 457 pp., Clarendon, Oxford, 1991.

Weast, R.C. (Ed.), *CRC Handbook of Chemistry and Physics*, 53rd ed, CRC Press, Boca Raton, Fla., 1973.

G.E. Ewing and D.D. Weis, Department of Chemistry, Indiana University, Bloomington, IN 47405. (e-mail: ewingg@indiana.edu; dweis@indiana.edu)

(Received August 9, 1995; revised May 2, 1996; accepted May 2, 1996.)